Self-Assembly of Star ABC Triblock Copolymer Thin Films: Self-Consistent Field Theory

Wenchi Han, Ping Tang,* Xuan Li, Feng Qiu, Hongdong Zhang, and Yuliang Yang

Key Laboratory of Molecular Engineering of Polymer, Ministry of Education, and Department of Macromolecular Science, Fudan University, Shanghai 200433, China

Received: February 26, 2008; Revised Manuscript Received: September 1, 2008

Microphase separation and morphology of star ABC triblock copolymers confined between two identical parallel walls (symmetric wetting or dewetting) are investigated with self-consistent field theory (SCFT) combined with the "masking" technique to describe the geometric confinement of the films. In particular, we examine the morphology of confined near-symmetric star triblock copolymers under symmetric and asymmetric interactions as a function of the film thickness and the surface field. Under the interplay between the degree of spatial confinement, characterized by the ratio of the film thickness to bulk period, and surface field, the confined star ABC triblock copolymers are found to exhibit a rich phase behavior. In the parameter space we have explored, the thin film morphologies are described by four primary classes including cylinders, perforated lamellae, lamellae, and other complex hybrid structures. Some of them involve novel structures, such as spheres in a continuous matrix and cylinders with alternating helices structure, which are observed to be stable with suitable film thickness and surface field. In particular, complex hybrid network structures in thin films of bulk cylinder-forming star triblock copolymers are found when the natural domain period is not commensurate with the film thickness. Furthermore, a strong surface field is found to be more significant than the spatial confinement on changing the morphology of star triblock copolymers in bulk. These findings provide a guide to designing novel microstructures involving star triblock copolymers via geometric confinement and surface fields.

Introduction

Block copolymers can self-assemble into a variety of ordered structures such as lamellae (LAM), hexagonally packed cylinders (HEX), and body-centered cubic (BCC) spheres and more complex structures such as gyroid (G) in melts and solutions.[1,2] This microphase separation has therefore attracted considerable attention in the area of soft condensed matter physics and nanotechnology.[3,4] In bulk, the morphology of block copolymers is determined mainly by the molecular architecture and the interaction between the different components.[2] However, thin film confinement has a great influence on the phase behavior of block copolymers,[5−7] and thus controlling the microdomain ordering in thin films has attracted much attention for polymer lithography. In comparison to the phase structure in bulk, two effects emerge in confinement. On the one hand, the commensurability of the natural microdomain spacing in bulk with the film thickness can impact the alignment of the structure; on the other hand, the preferential attraction of one type of the block to the surface (the surface field) will cause the surface segregation. By tuning the geometric confinement and the interactions between the polymers and the surfaces, a large scale alignment of a surface reconstruction and a series of complex morphologies can be obtained in thin films.[8,9]

Many studies have centered on the control of morphology of block copolymer systems under various confinements such as thin film,[8−14] cylindrical pore,[15−17] sphere,[18] and systems that involve the inclusion of filler particles.[19] Most theoretical studies on block copolymers in thin films have focused on two-component systems, either AB diblock[8−14,20] or symmetric ABA triblock copolymers,[20,21] which form lamellae or cylinders in bulk; details of these studies, including both experiments and theory, can be found in several reviews.[22−24] In contrast to two-component systems, the phase behavior of ABC triblock copolymers is expected to be more complex because the parameter space is much larger. Pickett et al.[25] used self-consistent field theory (SCFT) to probe the preferential orientation of lamellae formed by ABC linear triblock copolymers confined between two walls attracting the middle block: they found that an orientation of the lamellae perpendicular to the plane of the film is highly favored. Further, Monte Carlo simulations (MC) by Feng et al.[26] for linear ABC melts in thin films showed that the microphase separation was affected both by the composition and by the interactions between different species. Fredrickson et al.[27] applied self-consistent field theory (SCFT) and strong segregation limit (SSL) studies to investigate the confined films of linear ABC melts for the particular case where A and C block are equal in length under the symmetric interaction parameters between different species, and both walls have identical chemical properties. Liang et al.[28] studied the cylindrical structure formed in thin films of asymmetric composition linear ABC triblock copolymers with Monte Carlo simulations (MC) and observed transformations between parallel cylinders, perpendicular cylinders, and distorted mixed structures. The phase behavior of linear ABC triblock copolymers in thin films, which exhibits a core−shell gyroid structure in bulk, has been systematically studied by Ludwings et al.[29,30] in both mesoscale calculations and experiments. Numerous structures such as perpendicular cylinders, parallel cylinders, perforated lamellae, and core−shell gyroids have been identified. All these findings demonstrate that film thickness and surface fields can be employed to manipulate the microdomain structure, shape, and large-scale orientation, resulting in potentially functional microstructures.

Most of the present studies of ABC triblock copolymers in thin films have concerned on linear polymer chains. However,

* Corresponding author. E-mail: pingtang@fudan.edu.cn.

10.1021/jp801675z CCC: $40.75
Published on Web 10/11/2008

the properties of branched chains significantly differ from those of their linear analogues, particularly near interfaces and in confined geometries.[31] The simplest model of a nonlinear chain is a star polymer consisting of three arms attached to a mutual core (or junction point). Gemma et al.,[32] Tang et al.,[33] and Liang et al.[34,35] systematically investigated theoretically the morphology of star ABC triblock copolymer melts in bulk and found several stable microphases, including hexagonal lattice, core−shell hexagonal lattice, lamellae, and lamellae with cylinders. Moreover, they also found that when the volume fractions of the three species are comparable, the star architecture of the polymer chain imposes a strong topological constraint that regulates the geometry of the microphases, resulting in the formation of hexagonal honeycomb and even a polygon phase. Until present, however, only few reports concentrate on confined star-shaped polymers.[31,36]

In this work, we systematically evaluate the phase behavior of a system of star ABC triblock copolymers confined between two identical parallel walls by using self-consistent field theory (SCFT). SCFT has proved to be one of the most successful theoretical methods for investigating equilibrium phases in block copolymers and has played a major role in establishing the phase diagram of bulk block copolymer melts.[37,38] Matsen[11] first applied the SCFT of Helfand[39] to thin films of symmetric AB diblock copolymers and assumed that the total segment density rises continuously from zero to the bulk value within a distance (interface) from each wall based on the consideration of the total segment density would vanish on the confining walls. Wang et al.[40] evaluated the profiles at the interface using different functional forms and revealed that the choice of the profile strongly influences the numerical performance of the SCFT calculations. Fredrickson et al.[41] adopted a simple "masking" technique that confines the block copolymer between two walls by choosing a "masking" function to fit the geometry of the film. In this work, Fredrickson's masking trick is borrowed similarly to deal with the confinement effect of block copolymers and is extended to investigate the phase structure of star triblock copolymer thin films. In order to emphasize the significant topological constraint of star polymer chain on the morphology,[33] we conduct the simulation in the parameter space of almost symmetric volume fraction ($A_{0.3}B_{0.3}C_{0.4}$). The confinement effect on the phase behavior of system is thus systematically investigated as a function of film thickness and surface fields for three cases of Flory−Huggins interaction parameters.

Theoretical Method

In this section, we briefly describe the SCFT simulation method employed to predict the equilibrium structure of a system of confined star ABC triblock copolymers. We consider a system with volume V of n star triblock copolymers each having A, B, and C arms joined together at a center core, confined between two identical parallel walls. The total degree of polymerization of the star block is N, and the A, B, and C blocks consist of f_AN, f_BN, and f_CN monomers, respectively. We scale distances by the Gaussian radius of gyration: $R_g = a(N/6)^{1/2}$, where a is the monomer statistical Kuhn length. The bulk monomer density ρ is assumed to be same for all chemical species. We follow the "masking" technique proposed by Fredrickson et al.[41] to realize the confinement geometry of block copolymers between two walls. The main idea of this method is that a surface density field, $\phi_W(\mathbf{r})$ (W stands for wall, $0 < \phi_W(\mathbf{r}) < 1$), is introduced to confine the polymers into the region between two parallel film surfaces. The polymers are expelled by imposing an incompressibility constraint, namely, $\phi_A(\mathbf{r}) + \phi_B(\mathbf{r}) + \phi_C(\mathbf{r}) + \phi_W(\mathbf{r}) = 1$. Therefore, the choice of $\phi_W(\mathbf{r})$ determines the geometry of the film, and here we consider the two parallel walls normal to the z-axis with a hyperbolic tangent functional form:

$$\phi_W(\mathbf{r}_z) = \frac{1}{2}\left\{1 - \tanh\left[\frac{m}{t}\left(\frac{1}{2}(L_z - T) - \left|\mathbf{r}_z - \frac{1}{2}L_z\right|\right)\right]\right\} \quad (1)$$

where $L_z + 1$ is the length of system in the z direction of confinement. In fact, the expression of $\phi_W(\mathbf{r}_z)$ describes a planar cavity field centered at the xy-plane (symmetric about the midpoint of the system, namely $L_z/2$) with an overall cavity thickness T when the walls are separated by $L_z + 1$ lattice points; that is, $0 \le \mathbf{r}_z \le L_z$. Values of T should be reasonably chosen to prevent the overlap of the two interfaces; t is the interfacial thickness of the transition from inside to outside the cavity field, and in this work $0.5 \le t \le 1$ (R_g). The value of m should be chosen as $4 \le m \le 6$ to ensure that the value of tanh(···) can infinitely approach values of 1 and −1 as a function of film thickness. With decreasing t or increasing m, the interface becomes sharper, which is suitable for describing a small interfacial thickness. The film thickness d is expressed as the distance between two surfaces, that is, $d = (L_z + 1) - T$. In this way, the interior of the confinement film is set $\phi_W(\mathbf{r}_z) = 0$ and the exterior of the film is set $\phi_W(\mathbf{r}_z) = 1$ with a narrow and smooth transition region to connect the interior and exterior. We should note that the "masking" function adopted by us is similar to that used by Matsen[11] with the exception of different functional forms, such as cosine. In this paper, the hyperbolic tangent function can minimize the number of required Fourier modes needed to resolve the region ($0 < \phi_W(\mathbf{r}_z) < 1$) because the cosine function need much more lattice points to obtain, such as the same cavity thickness T, compared to the hyperbolic tangent function.[42] Furthermore, the confining wall is modeled as a fixed density field that interacts with the polymer segments via the incompressibility constraint and Flory−Huggins interactions.

In the SCFT model, one considers the statistics of a single copolymer chain in a set of effective chemical potential fields $\omega_i(\mathbf{r})$, where i represents block species A, B, and C. The free energy per chain may be calculated as

$$\frac{F}{nk_BT} = -\ln\left(\frac{Q}{V}\right) + \frac{1}{V}\int d\mathbf{r}(\chi_{AB}N\phi_A\phi_B + \chi_{BC}N\phi_B\phi_C + \chi_{AC}N\phi_A\phi_C) + \frac{1}{V}\int d\mathbf{r}(\chi_{AW}N\phi_A\phi_W + \chi_{BW}N\phi_B\phi_W + \chi_{CW}N\phi_C\phi_W) - \frac{1}{V}\int d\mathbf{r}(\omega_A\phi_A + \omega_B\phi_B + \omega_C\phi_C) - \frac{1}{V}\int d\mathbf{r}\xi(1 - \phi_A - \phi_B - \phi_C - \phi_W) \quad (2)$$

where χ_{ij} is the Flory−Huggins interaction parameter between different species i and j, χ_{iw} is dimensionless measures of the surface energy between species i and the walls, $\xi(\mathbf{r})$ is the relaxation parameter that ensures the incompressibility of the system, and V represents the effective volume occupied by copolymers: $V = \int d\mathbf{r}(1 - \phi_W(\mathbf{r}))$. $Q = \int d\mathbf{r}\, q_i(\mathbf{r},s)q_i^+(\mathbf{r},s)$ is the partition function of a single chain in the effective chemical potential field $\omega_i(\mathbf{r})$ and may be obtained by the polymer segment distribution function $q_i(\mathbf{r},s)$ for a single chain of contour length s with its end segment at position $\mathbf{r}$. Each star polymer

is parametrized with the variable s, which increases along each arm. The core of the star corresponds to $s = 0$; along the A arm, s increases from 0 at the core to $f_A N$ at the outer end. The B and C arms are parametrized similarly. $q_i(\mathbf{r},s)$ satisfies the modified diffusion equations[39]

$$\frac{\partial q_i(\mathbf{r},s)}{\partial s} = \frac{Na^2}{6}\nabla^2 q_i(\mathbf{r},s) - \omega_i(\mathbf{r})q_i(\mathbf{r},s)$$

$$\frac{\partial q_i^+(\mathbf{r},s)}{\partial s} = -\frac{Na^2}{6}\nabla^2 q_i^+(\mathbf{r},s) + \omega_i(\mathbf{r})q_i^+(\mathbf{r},s) \quad (3)$$

where $q_i^+(\mathbf{r},s)$ is another segment distribution function because the two ends of block copolymers are different. The initial conditions are $q_i(\mathbf{r},0) = q_j^+(\mathbf{r},0)q_k^+(\mathbf{r},0)$ and $q_i^+(\mathbf{r},f_iN) = 1$, where $(i, j, k) \in \{(A\ B\ C), (B\ C\ A), (C\ A\ B)\}$. $\phi_i(\mathbf{r})$ is the density of each block component and thus can be obtained:

$$\phi_A(\mathbf{r}) = -V\frac{\delta \ln Q}{\delta \omega_A} = \frac{V}{NQ}\int_0^{f_A N} \mathrm{d}s\, q_A(\mathbf{r},s)q_A^+(\mathbf{r},s) \quad (4)$$

$$\phi_B(\mathbf{r}) = -V\frac{\delta \ln Q}{\delta \omega_B} = \frac{V}{NQ}\int_0^{f_B N} \mathrm{d}s\, q_B(\mathbf{r},s)q_B^+(\mathbf{r},s) \quad (5)$$

$$\phi_C(\mathbf{r}) = -V\frac{\delta \ln Q}{\delta \omega_C} = \frac{V}{NQ}\int_0^{f_C N} \mathrm{d}s\, q_C(\mathbf{r},s)q_C^+(\mathbf{r},s) \quad (6)$$

According to mean-field approximation, minimization of the free energy with respect to densities and chemical potentials, namely, $\delta F/\delta\phi_i = \delta F/\delta\omega_i = 0$, leads to the following equations:

$$\omega_A(\mathbf{r}) = \chi_{AB}N\phi_B(\mathbf{r}) + \chi_{AC}N\phi_C(\mathbf{r}) + \chi_{AW}N\phi_W(\mathbf{r}) + \xi(\mathbf{r}) \quad (7)$$

$$\omega_B(\mathbf{r}) = \chi_{AB}N\phi_A(\mathbf{r}) + \chi_{BC}N\phi_C(\mathbf{r}) + \chi_{BW}N\phi_W(\mathbf{r}) + \xi(\mathbf{r}) \quad (8)$$

$$\omega_C(\mathbf{r}) = \chi_{AC}N\phi_A(\mathbf{r}) + \chi_{BC}N\phi_B(\mathbf{r}) + \chi_{CW}N\phi_W(\mathbf{r}) + \xi(\mathbf{r}) \quad (9)$$

$$\phi_A(\mathbf{r}) + \phi_B(\mathbf{r}) + \phi_C(\mathbf{r}) + \phi_W(\mathbf{r}) = 1 \quad (10)$$

Equations 3−10 form a closed set of self-consistent equations. The equations are numerically implemented by combinatorial screening algorithm proposed by Drolet and Fredrickson.[37,38] First, random initial values of field $\omega_i(\mathbf{r})$ are given. Second, the diffusion eqs 3 are solved to obtain $q(\mathbf{r},s)$ and $q^+(\mathbf{r},s)$ with the pseudospectral numerical method.[43] Third, the density fields are evaluated by eqs 4−6. Finally, with the obtained segment density, the fields $\omega_i(\mathbf{r})$ and $\xi(\mathbf{r})$ are updated by a combination of their old and new values according to eqs 7−10. With the new fields, the partition functions $q(\mathbf{r},s)$ and $q^+(\mathbf{r},s)$ are evaluated again to obtain the segment density. These steps are iterated until the free energy can converge to a stable value and the changes at each iteration are reduced to 10^{-5}, and the phase pattern emerging in the simulation box can be clearly identified.

The numerical simulations are conducted in three-dimensional space with $L_x \times L_y \times (L_z + 1)$ lattice with periodic boundary conditions in the x-, y-, and z-directions both in bulk and for the case of confinement. The system is confined between two walls separated by $L_z + 1$ lattice points. The discretization of the parameters is chosen to be $\Delta s = 1/100 = 0.01$; namely, the contour length is discretized 100 segments, the grid size $\Delta x = \Delta y = 0.245R_g$, and $\Delta z = 0.05R_g$ in this paper. We tested that this discretization in second-order pseudospectral method can ensure that the morphology is trustable. The free energy calculation converges rapidly and finally reaches the relative constant value (the free energy difference between two sequential iterations). To minimize the influence of the simulation box size in the x- and y-directions, each minimization of the free energy is iterated with respect to a variety of reasonable sizes ($5-8R_g$) in the x- and y-directions (L_x, L_y = 20, 22, 24, . . ., 32). In this work, the final stable phase is determined by comparing the free energies for at least 28 morphologies with the variation of the simulation box size in the x- and y-directions. We should note that this minimum obtained in this way in not necessarily a global minimum, and this can only be found by comparing the free energies of all saddle point solutions to the SCFT equations. In order to avoid the real space method sometimes becoming trapped in certain metastable states, random noises are added on the fields to disturb the morphology formed in the iterations. We should note that this method will not influence the final morphologies of the system according to comparing the free energy to determine the stable and metastable morphologies. Furthermore, all the minimization of the free energy is repeated several times by using different random initial states of fields $\omega_i(\mathbf{r})$ and different random numbers to guarantee that the structure is not occasionally observed. In this fashion, both typical ordered morphologies and the phase diagram for confined star ABC triblock copolymers can be obtained by systematically adjusting the values of the film thickness and surface field for different cases of Flory−Huggins interaction parameters.

Results and Discussion

Because of the complex parameter space for star ABC triblock copolymers,[32,33,35] especially in the case of the confinement, in our simulation, we choose a near-symmetric composition as $f_A = f_B = 0.30$ and $f_C = 0.40$ to emphasize the strong topological constraint of the star architecture of the polymer chain.[33] At first, we calculate the critical χN at ODT for symmetric interactions between the components for star $A_{0.3}B_{0.3}C_{0.4}$ triblock copolymers. The results show that at $\chi_{AB}N = \chi_{BC}N = \chi_{AC}N =$ 19.75 blocks A and B are mixed but separated with the C block; at $\chi_{AB}N = \chi_{BC}N = \chi_{AC}N = 21.55$, the A, B, and C blocks are completely separated. Therefore, $\chi N = 20$, $\chi N = 35$, and $\chi N =$ 50 can be regarded as corresponding to relatively weak-, intermediate-, or strong-segregation regime, respectively. In this study, the microphase structure is calculated for different values of Flory−Huggins interaction parameter $\chi N = (\chi_{AB}N, \chi_{AC}N, \chi_{BC}N)$. We first discuss the case with symmetric interaction parameters between three species as $\chi N = (35, 35, 35)$. We also focus on the influence of the asymmetry of the interaction parameters between the species on the phase behavior of star ABC triblock copolymers. To this effect, we consider two cases: we investigate conditions for which the interactions between block A and B are favorable than those between the AC and BC pairs, that is, $\chi N = (20, 50, 50)$; we further discuss more unfavorable interactions between blocks A and B such as $\chi N = (50, 20, 20)$. Obviously, the blocks A and B are symmetrically permutable relative to block C in the case of star ABC triblock copolymers. Regards the surface interactions, for simplicity, we assume that the surface walls are neutral to species A and B ($\chi_{AW}N = \chi_{BW}N = 0$) but have preference for the relative

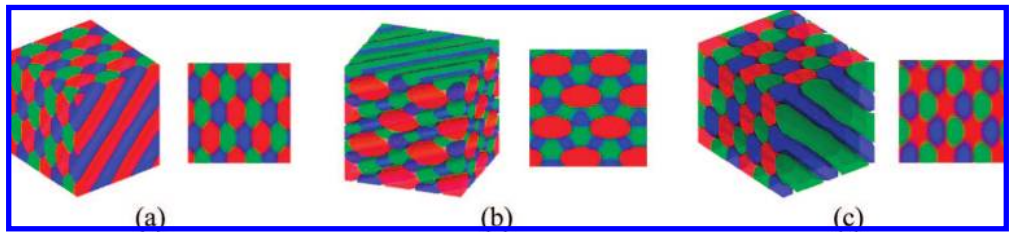

Figure 1. Equilibrium morphologies for star $A_{0.3}B_{0.3}C_{0.4}$ triblock copolymers in bulk. The blue, green, and red regions represent the density distributions of the monomers belonging to A, B, and C blocks, respectively. The interaction parameters between the components are $\chi N = (35, 35, 35)$ in (a), $\chi N = (20, 50, 50)$ in (b), and $\chi N = (50, 20, 20)$ in (c). The right pattern represents the density distribution profile of the projection of cylinders onto the cube face.

majority component C. The interaction parameter $\chi_{CW}N$ is varied in a wide range: a negative $\chi_{CW}N$ represents C-attractive wall while a positive $\chi_{CW}N$ means C-repellant surface wall.

A. Bulk Morphologies. To understand the change of microstructures induced by confining walls, we first depict the simulation results on the morphologies in bulk. The volume fraction are $f_A = f_B = 0.30$ and $f_C = 0.40$ ($A_{0.3}B_{0.3}C_{0.4}$) for the model system. Figure 1 shows the calculated self-assembled morphologies of star ABC triblock copolymers. Three different colors, blue, green, and red, are assigned to A, B, and C blocks, respectively. With symmetric interaction parameters as $\chi N = (35, 35, 35)$, we observe a three-component hexagonal honeycomb polygonal cylinder phase shown in Figure 1a, in agreement with that previously reported.[33] We note that each individual domain is hexagonal-like due to microphase separation between incompatible components with symmetric interaction parameter. Figure 1b reveals that as the interaction parameter is $\chi N = (20, 50, 50)$, the microstructure formed by the C block is a hexagonal elliptic cylinder phase. However, the polygonal cylinders formed by component A and B are packed in a pentagonal array. The domains of the A and B blocks are alternating hexagonal-like and tetragonal-like. This is expected, since components A (B) and C are highly incompatible and the domains are arranged in such a manner to a lower the surface energy between components C and two other components. By adjusting the interaction parameters to $\chi N = (50, 20, 20)$, as shown in Figure 1c, the microstructure of the system is also three-component hexagonal cylinder phase, but the domains of the A and B component are circle-like and only the domains formed by C blocks are hexagonal-like; the interfaces are somewhat diffuse because of relatively weaker repulsive interactions between these two components (A (B) and C). The circle-like domain with the minimum surface area therefore can reduce the contact area between the A and B components. These results are also consistent with the Monte Carlo simulations by Gemma et al.[32] and our previous 2D SCFT simulations.[33]

In bulk, as shown in Figure 1, the C-rich cylinders always exhibit hexagonal arranged for the three cases. The equilibrium periods cross two layers of the C-rich cylinders is found to be $L_1 \approx 6R_g$ for Figure 1a, $L_2 \approx 7.5R_g$ for Figure 1b, and $L_3 \approx 6.5R_g$ for Figure 1c, respectively. As pointed out by Wang et al.,[14] in the case of planar confinement, the frustration of the polymer period would reorient the cylinders' direction. Thus, in this paper, we order the self-assembled structures as a function of d/L_i (where d is the film thickness and $L_i (i = 1, 2, 3)$ is the equilibrium period for the C-rich cylinders in Figure 1a, Figure 1b, and Figure 1c, respectively) for describing confinement degree.

B. Thin Film Phase Behavior. Because the phase behavior of block copolymer films is primarily dictated by the interplay between the characteristic period of block copolymer microdomains and the film thicknesses as well as by the surface fields, we investigate the effect of the film thickness (spatial confinement) and surface field interactions for symmetric and asymmetric interaction parameters between different block species. Furthermore, the junction point limitation of star ABC triblock copolymers gives another entropic effect on polymer chains because the monomers must be gathered where the interfaces of three components meet.[32] A series of complex microphases are found including cylinders, undulated cylinders, perforated lamellae, lamellae, or hybrid network structures. In the parameter space we have explored, these morphologies are divided into four primary classes in terms of the phase behavior of relative majority component C: (1) cylinders, (2) perforated lamellae, (3) lamellae, and (4) complex hybrid structures with each class containing several kinds of related structures. The structures are shown in Figures 2−5.

1. C-Rich Cylinders. In contrast to the C-forming cylinders in bulk (Figure 1), four kinds of regular or irregular cylinders formed by component C are found in our screening, shown in Figure 2:

Perpendicular cylinders ($C_\perp$). In this case, the cylinders are aligned perpendicular to the surface walls including the following phases: $C_\perp$ 1: The three-component cylinders are packed in a hexagonal array. $C_\perp$ 2: The C-rich elliptic cylinders are packed in a hexagonal array with pentagonal array for A- and B-rich cylinders. $C_\perp$ 3: The three-component hexagonal cylinders with C-rich cylinders are slightly broadened at the surface (dumbbell-like structure). We note that most of these cylinders are very short, signifying that the upright cylinders always occur in very thin films within the explored parameter space.

Tilted cylinders. C_T: tilted three-component hexagonal cylinders.

Parallel cylinders ($C_{||}$). The cylinders are aligned parallel to the surface walls, including as follows. $C_{||}$ 1: The cylinders are the same array as $C_\perp$ 1 but parallel to the walls. $C_{||}$ 2: The cylinders are the same array as $C_\perp$ 2 but parallel to the walls. $C_{||}$ 3: C-rich cylinders with alternating A- and B-rich undulated cylinders oriented parallel to the film. $C_{||}$ 4: C-rich cylinders with alternating A- and B-rich single helices. $C_{||}$ 5: C-rich cylinders, A- and B-rich undulated cylinders with some degree of interconnections. $C_{||}$ 6: C-rich cylinders with network structures formed by alternating A- and B-rich twisted rods. $C_{||}$ 7: C-rich cylinders with A-rich cylindrical rods and B-rich network structures.

Undulated cylinders. C_U: C-rich undulated cylinders with network structures formed by alternating A- and B-rich beads.

2. C-Rich Perforated Lamellae Phase (PL). It is well-known that perforated lamellae structures in the bulk phase are metastable of diblock copolymers according to strong segregation theory[44] and SCFT.[45] Furthermore, to our knowledge, in studies of linear ABC triblock copolymer in bulk, the PL structures, including A/B stacked perforated lamellae and A/B/C stacked perforated lamellae, are also metastable phase.[46,47] Gemma et al. also suggested that the PL found in star ABC triblock

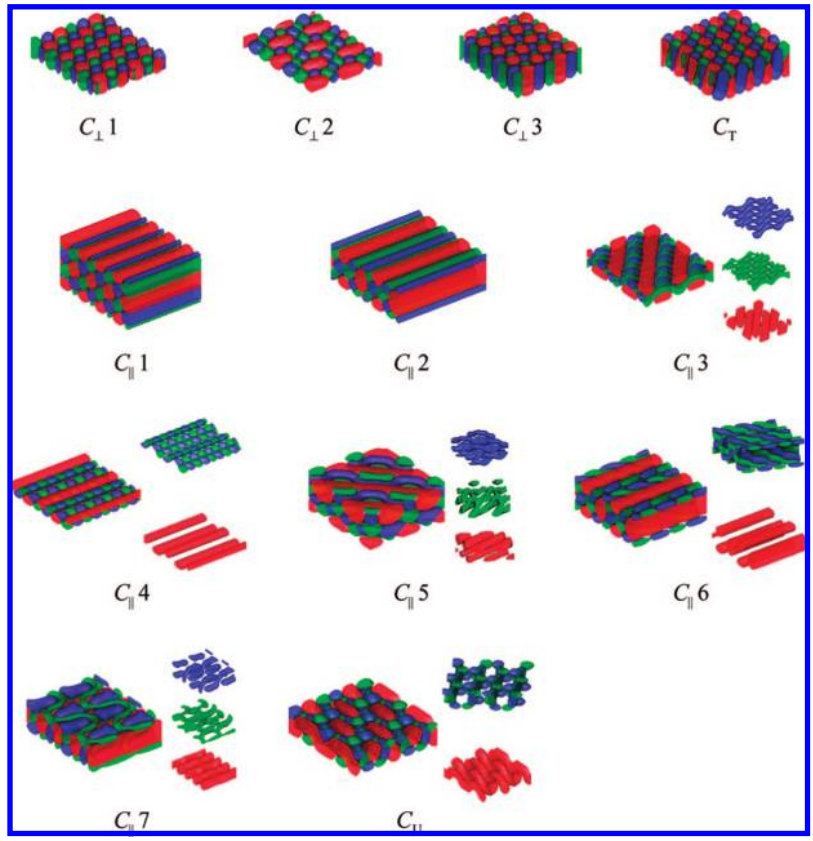

Figure 2. Representative structures of C-rich cylinder phases formed by star $A_{0.3}B_{0.3}C_{0.4}$ triblock copolymer thin films. The blue, green, and red regions represent isodensity surface distributions of the A, B, and C blocks, respectively.

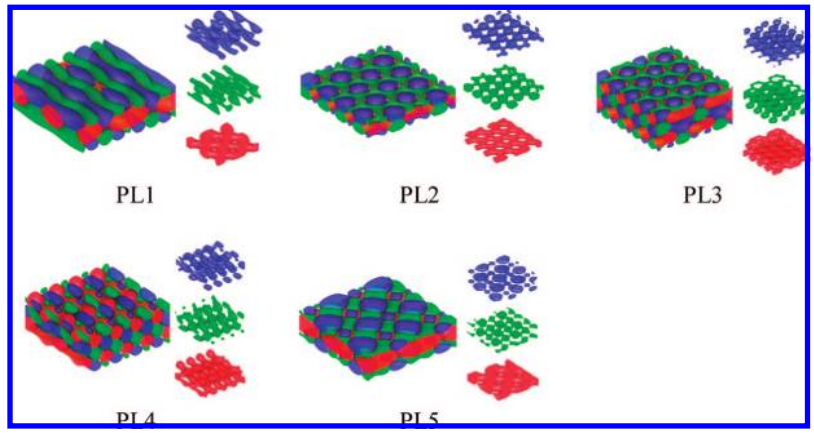

Figure 3. Representative structures of C-rich perforated lamellae phases formed by star $A_{0.3}B_{0.3}C_{0.4}$ triblock copolymer thin films. The blue, green, and red regions represent isodensity surface distributions of the A, B, and C blocks, respectively.

copolymer melts be not a true stable structure.[32] However, in this work, the PL structures formed by component C is stable under conditions with certain thicknesses and surface field, as shown in Figure 3. The perforated lamellae are also parallel to the surface, and in most situations, the pores are arranged in hexagonal array. PL1: C-rich perforated lamella between two layers formed by alternating A- and B-rich distorted cylinders with beads. PL2: C-rich perforated lamella between A- and B-rich perforated lamellae with alternating A- and B-rich beads inside the C block pores. PL3: B/C/C/A stacked perforated lamellae with alternating A- and B-rich undulated cylinders in the middle of the structure and alternating A- and B-rich beads inside the C block pores. PL4: C-rich undulated quadrangular perforated lamellae, A- and B-rich beads and undulated cylinders with some degree of interconnections. PL5: C-rich perforated lamella between two layers formed by alternating A- and B-rich cubic beads of different size packed in a quadrangular array with B-rich beads inside the C block pores.

3. C-Rich Lamellae Phase (L). As shown in Figure 4, several C-rich lamellae phases occur for asymmetric interactions between different polymer species due to confinement and surface field. These C-rich lamellae (L_C) are found always parallel to the walls, and a parallel layer formed by alternating A- and B-rich cylinders (L_{AB}) exists next to the L_C layer. L1: $L_{AB}/L_C/L_{AB}$ stacked lamellae. L2: $L_{AB}/L_C/L_{AB}/L_C$ stacked lamellae. L3: $L_{AB}/L_C/L_{ABC}$ stacked lamellae, where L_{ABC} is the mixture of C-rich cylinders with A- and B-rich undulated cylinders. We note that in L1 the cylinders of two L_{AB} layers are aligned with

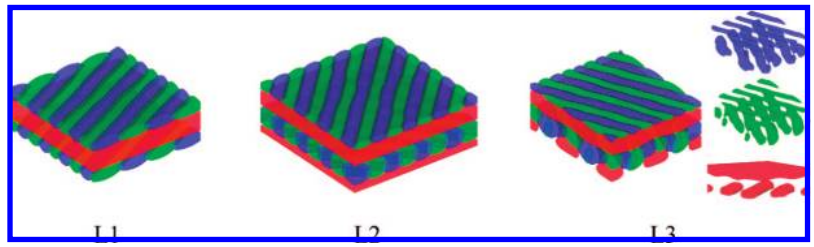

Figure 4. Representative structures of C-rich lamellae phases formed by star $A_{0.3}B_{0.3}C_{0.4}$ triblock copolymer thin films. The blue, green, and red regions represent isodensity surface distributions of the A, B, and C blocks, respectively.

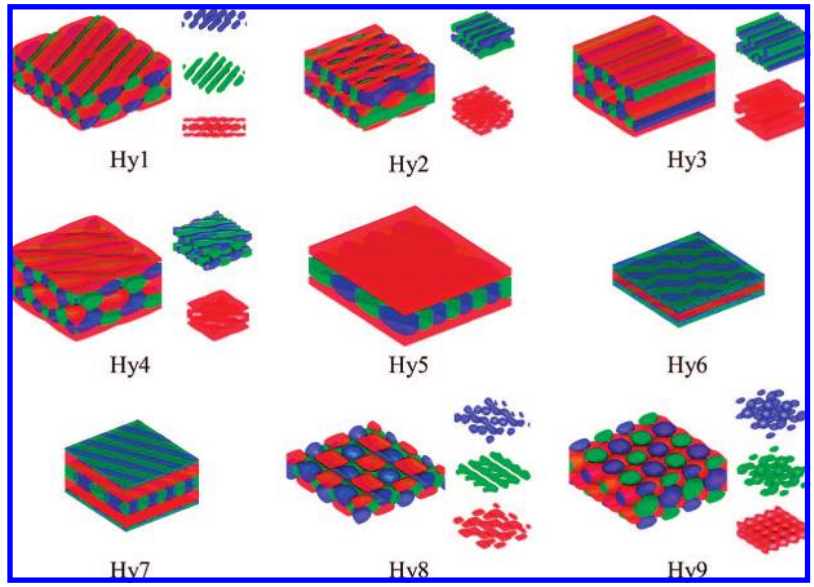

Figure 5. Representative hybrid structures formed by star $A_{0.3}B_{0.3}C_{0.4}$ triblock copolymer thin films. The blue, green, and red regions represent isodensity surface distributions of the A, B, and C blocks, respectively.

the same orientation, but in L2−L3 the orientation of the cylinders of L_{AB} layer is normal to that of another L_{AB} or L_{ABC} layer.

4. Complex Hybrid Structures. As shown in Figure 5, depending on the strength of the surface field, when $\chi_{CW}N$ is negative, i.e., the component C is preferentially attracted to the walls and the wetting layers at each surface are formed by the C block. Furthermore, when $\chi_{CW}N$ is positive, a weakly segregated AB thin layer in the vicinity of the surface walls occur, provided that there are relatively weaker repulsive interactions between the A and B blocks.

C-rich wetting layers. Hy1: the C-rich cylinders in the middle of the structure, and hexagonal array for A- and B-rich cylinders with two slightly fluctuating C-rich wetting layers. Hy2: C-rich perforated lamella between two layers formed by alternating A- and B-rich undulated cylinders with two C-rich wetting layers. Hy3: C-rich elliptic cylinders in the middle of the structure, and pentagonal array for A- and B-rich cylinders with two slightly fluctuating C-rich wetting layers. Hy4: C-rich slightly undulated cylinders in the middle of the film, and pentagonal array for A- and B-rich undulated cylinders with two slightly fluctuating C-rich wetting layers. Hy5: $L_C/L_{AB}/L_C$ stacked lamellae. In all these figures, on the top and bottom of the microphases, the C-rich layers exhibit cylinder-like, perforated lamellae-like, and lamellae-like structures, which we regard as wetting layers.

Weakly segregated AB layers. Hy6: C-rich lamella between two weakly segregated AB layers. Hy7: $L_C/L_{AB}/L_C$ stacked lamellae with two weakly segregated AB layers.

In addition, we find some novel structures of confined star ABC triblock copolymers shown in Figure 5. Hy8: C-rich cubic flat beads packed in a body-centered cubic array in a matrix formed by both A-rich undulated cylinders with beads and B-rich undulated cylinders with necks. Hy9: alternating cubic packed A- and B-rich spheres, analogous to a CsCl structure, inside a continuous matrix made of the C block.

The influence of the molecular architecture on the observed microstructures can be clearly distinguished by comparing our results with the behavior of linear ABC triblock copolymer under confinement studied by Pickett et al.[25] and Feng et al.[26] The simulation parameters such as interaction strength and copolymer composition are similar in both studies to facilitate the comparison. There is a significant difference between the phase behavior of confined linear ABC and star ABC triblock copolymers. For the case of symmetric interactions and copolymer compositions, only perpendicular and parallel lamellae phases are found in confined linear ABC system. By contrast, an array of complex and intricate structures emerges, in confined star ABC system, as shown in Figures 2−5.

C. For Neutral Walls. Both frustration effects by confinement and surface fields play important roles in polymer self-assembly process of thin films. To distinguish them, we first consider star ABC triblock copolymers to be confined between two parallel neutral walls that do not exert any preferential attraction on either polymer species ($\chi_{AW}N = \chi_{BW}N = \chi_{CW}N = 0$) for the sake of investigating the effect of confinement alone. The phase behavior is investigated by systematically varying film thickness with symmetric interaction parameters $\chi N = (35, 35, 35)$ as well as with asymmetric interaction parameters $\chi N = (20, 50, 50)$ and $\chi N = (50, 20, 20)$. Figure 6 shows the calculated phase diagrams corresponding to different values of χN with $\chi_{AW}N = \chi_{BW}N = \chi_{CW}N = 0$. Although similar

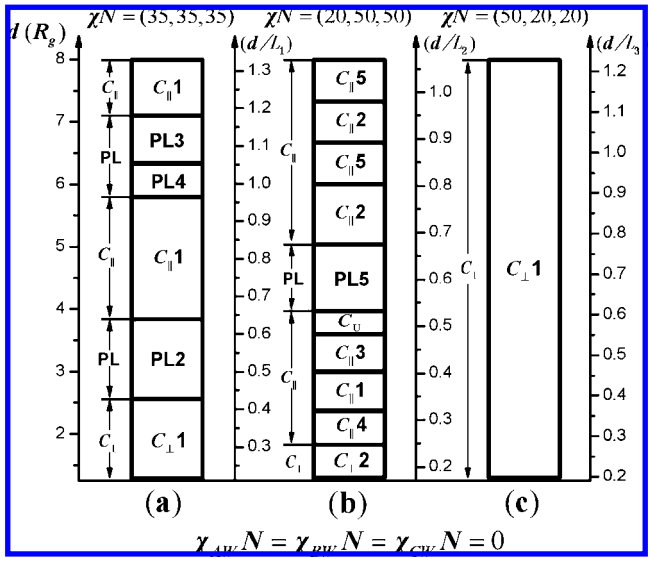

Figure 6. Phase diagram for star $A_{0.3}B_{0.3}C_{0.4}$ triblock copolymer thin films with neutral walls as a function of film thickness at symmetric and asymmetric interactions between polymer species. Squares indicate the range for each kind of morphology, shown in Figures 2−5. The interaction parameters between the components are $\chi N = (35, 35, 35)$ in (a), $\chi N = (20, 50, 50)$ in (b), and $\chi N = (50, 20, 20)$ in (c).

microphases are observed for different interactions in bulk, the presence of confining walls leads to significant changes in the phase behavior in contrast to Figure 1.

In Figure 6a, a phase diagram of confined star ABC triblock copolymer melts with symmetric interaction parameters $\chi N = (35, 35, 35)$ is established. With increasing film thickness, the region ($d/L_1 < 0.42$) of the film thickness shows perpendicular cylinders $C_\perp$ ($C_\perp$ 1), followed by perforated lamellae PL (PL2) ($0.42 < d/L_1 < 0.64$), parallel cylinders $C_\parallel$ ($C_\parallel$1) ($0.64 < d/L_1 < 0.96$), PL (PL4, PL3) ($0.96 < d/L_1 < 1.18$), and again $C_\parallel$ ($C_\parallel$1) ($d/L_1 > 1.18$) structures formed by the C block. We observe the $C_\parallel$ other than $C_\perp$ in thick films and therefore conclude that $C_\perp$ only occurs in very thin films. Suh et al.[20] investigated the ordering of cylindrical morphology in diblock and linear triblock copolymer thin films and concluded that the film thickness range in which the perpendicular morphology exists is not continuous and the range decreases with increasing thickness. They also reported that the perpendicular morphology cannot be found in thick films. Liang et al.[28] also suggested that the occurrence thickness range of perpendicular cylinder in linear triblock copolymer system decreases faster than that in diblock copolymers. The C-rich perforated lamellae (PL2, PL3, PL4) occur between the $C_\perp$ ($C_\parallel$) and $C_\parallel$ when the d/L_1 is about the integer or half an integer. A similar structural transition behavior was reported by Ludwigs et al.[29] with linear ABC triblock copolymer thin films. In fact, the PL structure is also widely found in diblock copolymer thin films[10] and linear ABA[21] and ABC[28,29] triblock copolymer thin films, but in these studies, the PL structure occurred only for confined system with surface field added. We conclude that the constraint of star junction point is the driving force for the formation of PL phases for star triblock copolymers under confinement without surface field. Furthermore, we note that in the PL structures the C-rich perforated lamellae cannot occur at the surfaces. In diblock copolymer thin film studies, Huinink et al.[13] found that for neutral walls there is a slight attraction for the shorter block and predicted this behavior as entropic preference. A similar phenomenon was also observed by Wang et al.[14] with Monte Carlo simulations and Yang et al.[10] with SCFT calculations. They attributed this effect to the enrichment of the chain ends (relative to middle segments) near the surface.

For the case of asymmetric interaction parameters $\chi N = (20, 50, 50)$, Figure 6b shows the morphologies of confined star ABC triblock copolymers as a function of the film thickness. As the film thickness increases, the C block forming phases follow the sequence from $C_\perp$ ($C_\perp$ 2) ($d/L_2 < 0.25$), to $C_\parallel$ ($C_\parallel$ 4, $C_\parallel$ 1) ($0.25 < d/L_2 < 0.4$), to undulated $C_\parallel$ ($C_\parallel$ 3, C_U) ($0.4 < d/L_2 < 0.53$), to PL (PL5) ($0.53 < d/L_2 < 0.68$), and to $C_\parallel$ ($C_\parallel$ 2, $C_\parallel$ 5) ($d/L_2 > 0.68$) again. From Figure 6b, a large region of parallel cylinders formed by the C block emerges under confinement due to the strong incompatibility between component C and component A (B). In particular, when the d/L_2 is about the integer or half an integer, complex network structure and undulated cylinders (strongly deformed) formed by the A and B blocks ($C_\parallel$ 3, C_U, $C_\parallel$ 5) are found due to the coupling effects of confinement and star architecture. In this case, the A-rich and B-rich cylinders are easily deformed under confinement because of the relative weak interaction between blocks A and B ($\chi_{AB}N = 20$); meanwhile, the C-rich cylinders are adjusted to highly deformed A-rich and B-rich cylinders under the constraint of star junction point. Similar undulated cylinders were reported by Lyakhova et al.[21] for the linear ABA triblock copolymer thin films under asymmetric surface field and by Yang et al.[10] with diblock copolymer thin films under symmetric surface field. However, in our study, the undulated cylinder structures occur for both neutral walls and walls with the surface field (see the next section). On the one hand, the cylinders are contorted to adapt to the film thickness while doing the best to minimize the unfavorable contacts with other components and walls. On the other hand, the junction point limitation gives another entropic effect in star triblock copolymers, resulting in the shape modulation of cylinders.

In Figure 6b, at $0.25 < d/L_2 < 0.31$, a novel structure that C-rich cylinders with alternating A- and B-rich single helices ($C_\parallel$ 4 in Figure 2) is induced. Although helical structures were reported by Feng et al.[48] with linear ABC triblock copolymer confined in nanocylindrical tubes and by Yu et al.[17,49] with diblock copolymer confined in channels of various shapes, as well as by Breiner et al.[50] with bulk linear ABC triblock copolymer studies, to our knowledge, such a structure have not been reported before. Because of the constraint of star junction point, the helices formed by A and B block are alternative and confined between C-rich cylinders.

Figure 6c shows the microphases corresponding to different film thicknesses with asymmetric interaction parameters $\chi N = (50, 20, 20)$. In contrast to Figure 6a,b, only the $C_\perp$ phase ($C_\perp$ 1 in Figure 2) is found at the whole range of the film thickness. It is noted that the perpendicular phase is always stable as the film thickness varies with the confined symmetric diblock copolymer melts for neutral walls.[10,11,14] By comparing the results of confined AB diblock copolymer[10−12,14] and ABA triblock copolymer melts,[21] the reason for this behavior can be qualitatively understood. Since the interaction between components A and B is more unfavorable for $\chi N = (50, 20, 20)$, in this case, the phase behavior is similar to that of AB diblock copolymers, which always exhibits perpendicular phases for neutral walls without entropic preference.[10,11]

From Figure 6, we conclude that for the case of neutral walls the cylinder forming phases from block C (are shown in Figure 2) is the prevalent structure in a wide range of film thickness. Furthermore, under the star junction point constraint, the A and B blocks also tend to form cylinder structures, whose radius and shapes are quite flexible in order to accommodate different

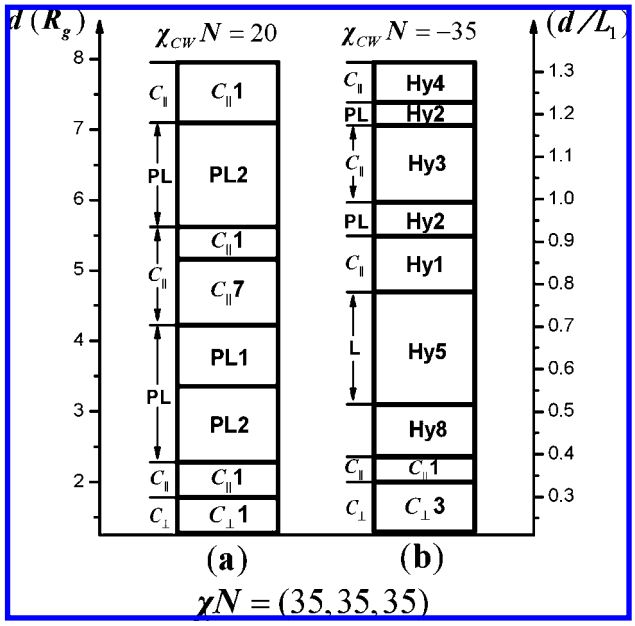

Figure 7. Effect of the surface field on the phase diagram for star $A_{0.3}B_{0.3}C_{0.4}$ triblock copolymer thin films with $\chi N = (35, 35, 35)$ as a function of film thickness. Squares indicate the range for each kind of morphology, shown in Figures 2−5. The interaction parameters between the C block and the walls are $\chi_{CW}N = 20$ in (a) and $\chi_{CW}N = -35$ in (b).

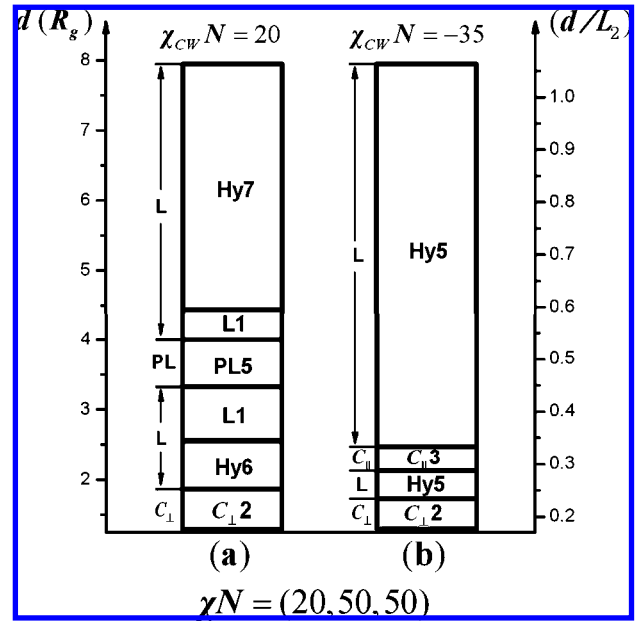

Figure 8. Effect of the surface field on the phase diagram for star $A_{0.3}B_{0.3}C_{0.4}$ triblock copolymer thin films with $\chi N = (20, 50, 50)$ as a function of film thickness. Squares indicate the range for each kind of morphology, shown in Figures 2−5. The interaction parameters between the C block and the walls are $\chi_{CW}N = 20$ in (a) and $\chi_{CW}N = -35$ in (b).

film thicknesses. Similar phenomena of the cylinder phase have been reported by Lyakhova et al.[21] with confined linear ABA systems and Ludwigs et al.[29] with confined linear ABC systems.

D. For Preferential Walls. We further study the effect of the surface field on the microstructures of the confined star ABC triblock copolymers as a function of film thickness. We consider two situations corresponding to repulsive ($\chi_{CW}N = 20$) and strongly attractive ($\chi_{CW}N = -35$) surfaces for the C block. For symmetric interaction parameters $\chi N = (35, 35, 35)$, the phase diagram is shown in Figure 7. Figure 7a corresponds to $\chi_{CW}N = 20$; i.e., the walls have an repellent effect for the C block. Figure 7b is for $\chi_{CW}N = -35$; namely, the walls have an effective attraction for the C block. By comparing Figure 6a (for neutral walls) and Figure 7a, we observe that there is a similar tendency toward the transformation of microstructures with the increase of the film thickness. However, the phase boundary is slightly shifted upon the incorporation of the surface field. When the surface walls have repulsion for the C block, $C_\perp$ structures can be obtained only at very thin films ($d/L_1 < 0.29$). We also observe that the range of PL phase becomes large after the surface filed is introduced. In Figure 7b, with an effective attraction for the C block, we find that the $C_\perp$ phase occurs at the small thickness; in this case, the C-rich cylinders are broadened at the surface in an attempt to wet the surface ($C_\perp$ 3 in Figure 2). As the film thickness increases, the $C_\parallel$ structure replaces the $C_\perp$ phase, and the C-rich wetting layers at the surface are induced due to the attraction of the surface walls to the block C. With further increasing the film thickness, the morphologies of C-rich wetting layer are transformed to beads (Hy8), to lamellae (Hy5), to compressed cylinders (Hy1), to perforated lamellae (Hy2), and to slightly fluctuating lamellae (Hy3, Hy4). The interior structures of these morphologies consist of a matrix formed by complex AB hybrid structure (Hy8), the layer formed by alternating A- and B-rich cylinders (Hy5), the alternating A- and B-rich undulated cylinders with C-rich PL phase (Hy2), and cylinders (Hy1, Hy3, Hy4). The C block in the middle of the structures where the surface field becomes less important tends to form perforated lamellae or cylinders (Hy1−Hy4).

Figure 8 shows the phase behavior for $\chi N = (20, 50, 50)$. Figure 8a corresponds to $\chi_{CW}N = 20$ and Figure 8b to $\chi_{CW}N = -35$. We observe that after the surface field is added, the C-rich lamellae phase becomes dominant in all equilibrium morphologies (L1, Hy5−Hy7). In Figure 8a, with increasing film thickness, the sequence of microphase transformation is from C-block $C_\perp$ ($C_\perp$ 2) ($d/L_2 < 0.24$), to L (Hy6, L1) ($0.24 < d/L_2 < 0.45$), to PL (PL5) ($0.45 < d/L_2 < 0.53$), and again to L (L1, Hy7) ($d/L_2 > 0.53$). We find that the AB layers are formed not only by alternating A- and B-rich cylinders but also by a weakly segregated AB layer at the surface (Hy6, Hy7). Because in this case the C block is repelled away from the walls, a small quantity of the A and B block will be gathered at the surface to form a thin layer when blocks A and B are weakly incompatible at certain film thicknesses. From Figure 8a, although the blocks A and B are weakly incompatible, a weakly segregated AB layer is found at the surface (Hy6, Hy7) but not at all the film thickness, and clear microphase separation of blocks A and B (PL5, L1) is found at certain film thicknesses. Moreover, the weakly segregated AB layers disappear in the center of the film since the surface field is weak. In quite thick films, only the weakly segregated AB layers (Hy7) at the surface are found in a large thickness range. This intriguing finding reveals that the confinement and surface field can affect the degree of microphase separation.

Figure 8b shows the transformation of microstructures as a function of the film thickness when the walls have an effective attraction for the C block. We observe the following structures as the film thickness increases: the C-block $C_\perp$ ($C_\perp$ 2) ($d/L_2 < 0.23$), L (Hy5) ($0.23 < d/L_2 < 0.28$), $C_\parallel$ ($C_\parallel$ 3) ($0.28 < d/L_2 < 0.33$), and again L (Hy5) ($d\,L_2 > 0.33$). In a large film thickness range, the C-rich lamellae structure is obtained with homogeneous wetting layers formed by the C block at the surface due to the attraction of the walls to the C block.

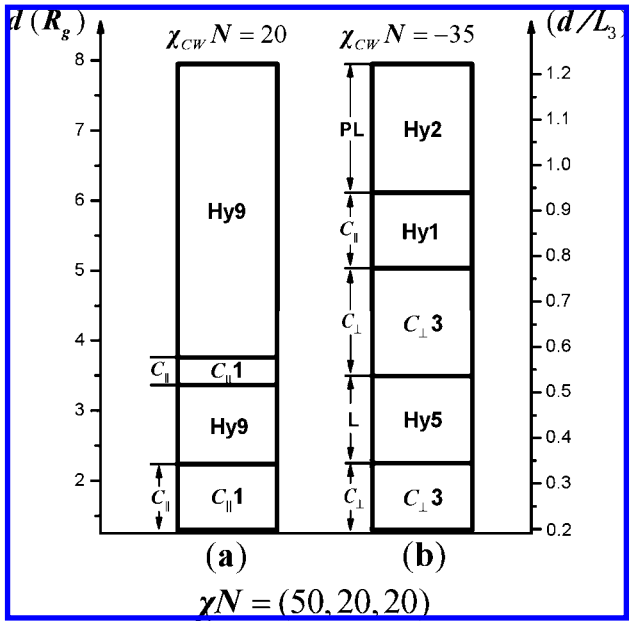

Figure 9. Effect of the surface field on the phase diagram for star $A_{0.3}B_{0.3}C_{0.4}$ triblock copolymer thin films with $\chi N = (50, 20, 20)$ as a function of film thickness. Squares indicate the range for each kind of morphology, shown in Figures 2−5. The interaction parameters between the C block and the walls are $\chi_{CW}N = 20$ in (a) and $\chi_{CW}N = -35$ in (b).

We now turn to the microphase structures in the center of the film. From Figure 8a,b, we find that in relatively thick films, while the effect of surface field becomes less important, lamellae with cylinders ($L_C + L_{AB}$) occur in the center of the film at large film thickness range, in contrast to the case of neutral walls. In lamellae with cylinders structure, the domain spacing is relatively small compared to the bulk structure and the effect of star junction point to the structure becomes less important, thus leading to lamellae with cylinders structure in a relatively large film thickness range. In fact, lamellae with cylinders have been reported by Gemma et al.[32] and Tang et al.[33] in bulk star triblock copolymers with the volume fraction ratio of N_A:N_B:N_C = 1:1:3−5 for symmetric interactions. This suggests that it might be possible to modulate the morphologies of the bulk copolymers by placing them under confinement and imposing prescribed surface fields.

Figure 9 shows the phase behavior as a function of the film thickness for $\chi N = (50, 20, 20)$. When $\chi_{CW}N = 20$, i.e., the C block has a strong repulsion from the walls, depicted in Figure 9a, the C-block $C_\perp$ phase does not exist even at small film thickness. As Suh et al.[20] pointed out, a perpendicular cylinder structure in very thin films is energy favored, in qualitative agreement with our calculations. However, an orientation of the microphases parallel to the surface is found in very thin films when $\chi_{CW}N = 20$ and $\chi N = (50, 20, 20)$. As film thickness increases, the C block $C_\parallel$ phase ($C_\parallel$ 1) ($d/L_3 < 0.35$, $0.52 < d/L_3 < 0.58$) and alternating cubic packed A- and B-rich spheres, analogous to a CsCl structure, inside a continuous matrix made of the C block (Hy9) ($0.35 < d/L_3 < 0.52$, $d/L_3 > 0.58$) occurs in turn. The structure (Hy9), reported by Bates et al.[46] with linear nonfrustrated ABC triblock copolymers in bulk, is found to occur at a large film thickness range; this is because the domain spacing is relatively small compared to the bulk structure and the influence of star junction point on the structure period becomes less important. When the walls have an effective attraction for the C block at $\chi_{CW}N = -35$, shown in Figure 9b, with increasing the film thickness, the phase sequence follows C-block perpendicular cylinders, broadened at the interface ($C_\perp$ 3) ($d/L_3 < 0.35$), lamellae phase (Hy5) ($0.35 < d/L_3 < 0.54$), again $C_\perp$ 3 phase ($0.54 < d/L_3 < 0.78$), cylinders with wetting layers (Hy1) ($0.78 < d/L_3 < 0.94$) and perforated lamella with wetting layers (Hy2) ($d/L_3 > 0.94$). In contrast to the C-block perpendicular cylinders ($C_\perp$ 1) appeared in the case of neutral walls in Figure 6c, the $C_\perp$ 3 structure is somewhat different, in which the C-block cylinders are slightly broadened at the surface to form dumbbell-like structure. We note that the wetting layers formed by C-rich cylinders and perforated lamellae are highly compressed such as Hy1 and Hy2 at the surfaces, and the A and B blocks always form cylinder-like structures in Figure 9b.

E. Influence of the Strength of the Surface Field. In this section, we will investigate how the film phase behavior is influenced by the strength of the surface field. For the sake of clarity, we only consider the case for interaction parameters $\chi_{AW}N = \chi_{BW}N = 0$ and $\chi_{CW}N$ spanning the range from repulsive to strongly attractive surfaces. First, we present the effect of the surface field for relative thinner films, such as $d = 2.5R_g$, and thus both the effects of the confinement and surface field are significant. Figure 10 shows the phase diagrams of films with different interaction parameters between different polymer species. For the case of $\chi_{CW}N = 0$, the $C_\perp$ phase ($C_\perp$ 1) is found for $\chi N = (35, 35, 35)$ and $\chi N = (50, 20, 20)$, whereas $C_\parallel$ structure ($C_\parallel$ 1) occurs for $\chi N = (20, 50, 50)$. As the attractive effect of the wall for component C ($\chi_{CW}N < 0$) increases, the $C_\parallel$ phase (C_U, $C_\parallel$ 3) will replace the $C_\perp$ with the A and B blocks gradually expelled form the surfaces, since the $C_\perp$ costs too many elastic energies to wet the surface.[41] When the attractive effect of the wall for component C increases further, the walls are mainly occupied by the C block to form a C-rich wetting layer (Hy5). When the repulsive effect of the wall for component C ($\chi_{CW}N > 0$) increases, the $C_\perp$ phase also disappears, and the C block is gradually transferred to the center of the film (PL2, Hy6, and Hy9). As the strength of the surface field increases, some noncylindrical structures formed by the C block are obtained. For example, the $C_\parallel$ phase tends to be transformed to beads (Hy8), to perforated lamellae (PL2), to lamellae (Hy5, Hy6), or to the alternating versions of the sphere structure (Hy9). For symmetric interactions $\chi N = (35, 35, 35)$, shown in Figure 10a, the cylinder phases occur in a large range of $\chi_{CW}N$ in comparison to the case of asymmetric interactions in Figure 10b,c. Some noncylindrical structures (PL2, Hy5, Hy8) are found at $\chi_{CW}N > 19$ and $\chi_{CW}N < -27$. In Figure 10b, a decrease of the repulsion between the A and B species leads to weakly segregated AB layers (Hy6) at $\chi_{CW}N > 3$, and the C-rich lamellae phases (Hy5, Hy6) are found at $\chi_{CW}N > 3$ or $\chi_{CW}N < -23$. However, in Figure 10c, the more unfavorable interaction between the A and B species leads to the result that the $C_\perp$ phase ($C_\perp$ 1, $C_\perp$ 3) can be obtained in a large range of $\chi_{CW}N$, and the noncylindrical structures (Hy5, Hy9) occur at $\chi_{CW}N > 7$ and $\chi_{CW}N < -25$. From Figure 10, we observe that the structural transition as a function of $\chi_{CW}N$ is more complex for symmetric interactions between polymer species, and the increase of strength of the surface field, i.e., the increase of the absolute value of $\chi_{CW}N$, results in C-block noncylindrical structures.

We further study the effect of the surface field on the phase behavior in relatively thick films, such as $d = 5.5R_g$. In this case, therefore, there is a lack of the impact of the surface field to the center of the films. The phase diagrams of confined star ABC triblock copolymers for different interactions between polymer species as a function of $\chi_{CW}N$ is shown in Figure 11. For the case of neutral walls, the $C_\parallel$ phase ($C_\parallel$ 1, $C_\parallel$ 2) is

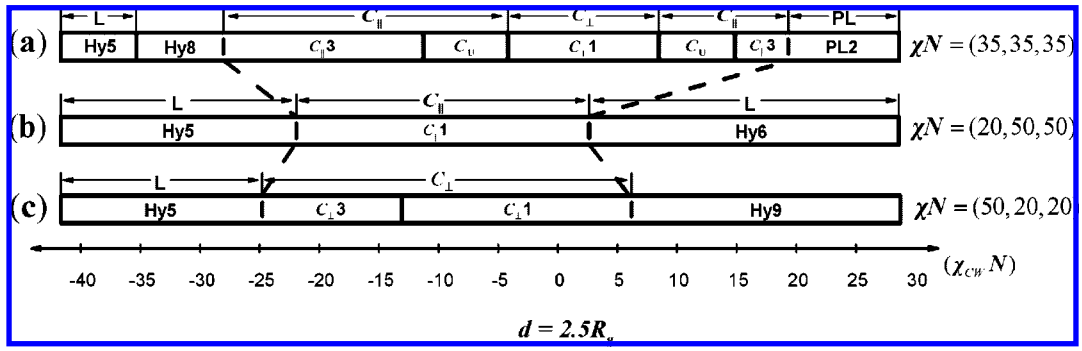

Figure 10. Morphology stability regions for star $A_{0.3}B_{0.3}C_{0.4}$ triblock copolymer thin films as a function of the surface field $\chi_{CW}N$ at $d = 2.5R_g$. Squares indicate the range for each kind of morphology, shown in Figures 2−5. The dashed lines indicate the structural transition between cylinders and noncylindrical phases for C block. The interaction parameters between the components are $\chi N = (35, 35, 35)$ in (a), $\chi N = (20, 50, 50)$ in (b), and $\chi N = (50, 20, 20)$ in (c).

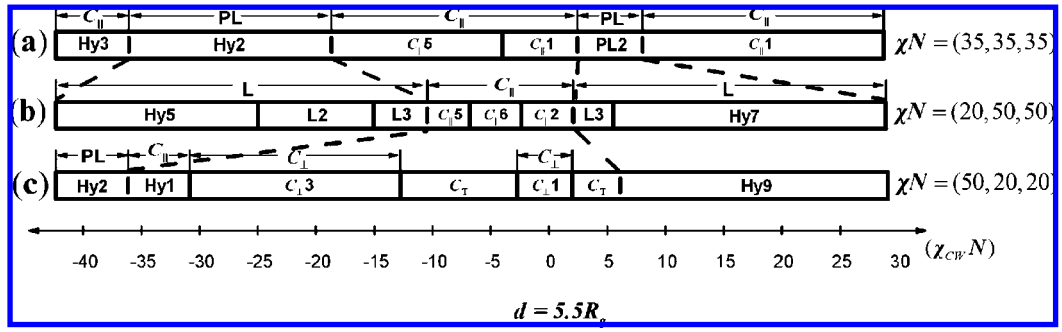

Figure 11. Morphology stability regions for star $A_{0.3}B_{0.3}C_{0.4}$ triblock copolymer thin films as a function of the surface field $\chi_{CW}N$ at $d = 5.5R_g$. Squares indicate the range for each kind of morphology, shown in Figures 2−5. The dashed lines indicate the transition between cylinders and noncylindrical phases for C block. The interaction parameters between the components are $\chi N = (35, 35, 35)$ in (a), $\chi N = (20, 50, 50)$ in (b), and $\chi N = (50, 20, 20)$ in (c).

observed for $\chi N = (35, 35, 35)$ and $\chi N = (20, 50, 50)$, whereas the $C_\perp$ structure ($C_\perp$ 1) is found for $\chi N = (50, 20, 20)$. In Figure 11a, for symmetric interactions, with increasing the strength of the surface field, we observe the C-rich PL structures (PL2, Hy2) in a certain range of $\chi_{CW}N$. With a further increase of the strength of the surface field, the C block cylinder phases ($C_\parallel$ 1, Hy3) occur again. This behavior is similar to the results in Figures 6a and 7 obtained by tuning the film thickness at the fixed value of the surface field for symmetric interactions between polymer species. Figure 11b reveals that depending on the strength of the surface field, the structural transition is more complex for the weaker repulsive between component A and B. It is found that the cylinder phases ($C_\parallel$ 2, $C_\parallel$ 5, $C_\parallel$ 6) exist in a relatively small range of $\chi_{CW}N = -10$ to 3, namely weak surface fields, and the C-rich lamellae phases (L2, L3, Hy5, Hy7) occur as the strength of the surface field increases. When the walls have an attraction for the C block ($\chi_{CW}N < 0$), the C-rich cylinders ($C_\parallel$ 5, $C_\parallel$ 6) remain at small value of $\chi_{CW}N$, but with the increase of the attraction of walls for the C block, the C-rich cylinders are gradually transferred to the surface and the complex hybrid structures with undulated cylinders or rods are formed. With increasing the surface field continuously, we find that the $C_\parallel$ phase is replaced by the C-rich lamellae phase, and moreover, some new structures between the lamellae and cylinders occur, such as asymmetric lamellar with cylinder phase (L2), and a coexistence of C-rich lamella and cylinder phase (L3). This behavior is attributed to the interplay between the surface field and the incommensurability between the optimal period of the lamellae phase and the film thickness. When the strength of the surface field is large enough ($\chi_{CW}N > 6$ and $\chi_{CW}N < -25$), the C-rich lamellae structures (Hy5 and Hy7) are stable even by further increasing the strength of the surface field. This phenomenon illuminates us that the surface field can modulate the microdomain periodicity of thin films. In Figure 11c, in the case of quite unfavorable interaction between blocks A and B, a tilted cylinder phase (C_T) occurs at small absolute values of $\chi_{CW}N$ and then is transformed to perpendicular cylinders with C-rich cylinders broadened at the interface ($C_\perp$ 3) or C-rich matrix phase (Hy9) with the increase of absolute values of $\chi_{CW}N$. The noncylindrical structures (Hy2 and Hy9) occur at $\chi_{CW}N > 7$ and $\chi_{CW}N < -36$.

By comparing Figures 10 and 11, we observe that when the surface field is weak, the cylinder phases are frequently observed because the confinement effect is dominant. When the surface field is strong enough, the surface field dominates film morphologies over spatial confinement. The same behavior was observed in studies of copolymers confined both in thin films[10,12,14,21,28] and in cylindrical nanopores.[17,18,48,51] Moreover, the surface field can break up the cylinder structure, and a variety of noncylindrical structures become favored. In particular, the noncylindrical structures are preferred for asymmetric interactions between polymer species and high strength of the surface field. In thinner films with symmetric interactions, noncylindrical structures are also found at high surface field strength (Figure 10a) since both effects of the confinement and surface field are significant in this case. However, in relatively thick films, the symmetric interactions between polymer species lead to the existence of the cylinder phases ($C_\parallel$ 1, Hy3) even for high strength of the surface field (Figure 11a). We also find that in relatively thick films the structural transition becomes more complex, and the strength of surface field needed to form noncylindrical microdomains decreases because the effect of the surface field on the center of thin films becomes less important. In both thin and thick films, when the value of $\chi_{CW}N$ is large enough,

the film structure seems to be stable with further increasing $\chi_{CW}N$. From the above findings, we can conclude that strong surface field is more powerful in tuning the phase structure in bulk than spatial confinement.

Conclusions

We have described the complex phase behavior of a model star ABC triblock copolymers confined between two identical parallel walls. The volume fraction of three different polymer species is chosen to be near-symmetric to emphasize the effect of the star architecture of the polymer chain in regulating the geometry of the microphases formed. By systematically changing the film thickness and the surface field, the self-assembled structures of confined star ABC triblock copolymer melts with the symmetric and asymmetric interactions between polymer species are carried out by SCFT simulations.

A variety of structures are found to be stable under the confinement and surface field conditions, such as cylinders, undulated cylinders, lamellae with cylinders, perforated lamellae, and alternating versions of the sphere in matrix structures, etc. For the case of neutral walls, the constraint of star chain architecture has an important effect on film morphologies. As a result, cylinder or cylinder-like structures are commonly observed in thin films, similar to the bulk morphologies. Moreover, the cylinder radius and shapes are found to be quite flexible in order to adjust themselves to different film thicknesses. In particular, some new morphologies, such as alternating helices between cylinders and complex hybrid network structures, not yet reported in the previous investigation for either AB diblock and linear ABC triblock copolymer films, are found in our explored parameter space. When the walls prefer one block of the copolymers, some interesting morphologies at the surface are induced, such as weakly segregated AB layers and C-rich wetting layers. The appearance of these structures effectively reduces the effect of surface field on the morphologies of the center film. In general, for weak surface fields, the cylinder-like structures are commonly observed; the confinement and commensurability between the microdomain periodicity and the film thickness may play a major role in controlling the structure of films. However, sufficiently strong surface fields can induce a transformation from cylindrical phases to noncylindrical structures, and the effect of constraint of star chain architecture on the phase behavior under confinement is weakened.

In particular, the confined star triblock copolymers are more sensitive to interaction parameters between polymer species, in comparison to the bulk. Cylinder structures and perforated lamellae phases occurring at well-defined film thickness are observed for symmetric interactions. For asymmetric interactions, the surface field can easily break up cylinder structures, and a variety of noncylindrical structures are favored. Our simulation results may provide a guide to understanding the complex interplay between star chain architecture, confinement effects, surface field, and interaction parameters in thin films of star triblock copolymers.

Acknowledgment. We thank financial support from the National Basic Research Program of China (Grant 2005CB623800) and for the Outstanding Research Group Project of NSF of China. Funding from the NSF of China (Grants 20474012, 20374016, and 20104002) is also acknowledged. We also thank J. T. Cabral for reading the manuscript at Imperial College as a visiting scholar in Fudan University.

References and Notes

(1) Bates, F. S.; Fredrickson, G. H. *Annu. Rev. Phys. Chem.* **1990**, *41*, 525.
(2) Bates, F. S.; Fredrickson, G. H. *Phys. Today* **1999**, *52*, 32.
(3) Matsen, M. W. *J. Phys.: Condens. Matter* **2002**, *14*, R21.
(4) Park, M.; Harrison, C.; Chaikin, P. M.; Register, R. A.; Adamson, D. H. *Science* **1997**, *276*, 1401.
(5) Lambooy, P.; Russell, T. P.; Kellogg, G. J.; Mayes, A. M.; Gallagher, P. D.; Satija, S. K. *Phys. Rev. Lett.* **1994**, *72*, 2899.
(6) Turner, M. S. *Phys. Rev. Lett.* **1992**, *69*, 1788.
(7) Turner, M. S.; Rubinstein, M.; Marques, C. M. *Macromolecules* **1994**, *27*, 4986.
(8) Kellogg, G. J.; Walton, D. G.; Mayes, A. M.; Lambooy, P.; Russell, T. P.; Gallagher, P. D.; Satija, S. K. *Phys. Rev. Lett.* **1996**, *76*, 2503.
(9) Walton, D. G.; Kellogg, G. J.; Mayes, A. M.; Lambooy, P.; Russell, T. P. *Macromolecules* **1994**, *27*, 6225.
(10) Yang, Y. Z.; Qiu, F.; Zhang, H. D.; Yang, Y. L. *Polymer* **2006**, *47*, 2205.
(11) Matsen, M. W. *J. Chem. Phys.* **1997**, *106*, 7781.
(12) Wang, Q.; Yan, Q. L.; Nealey, P. F.; de Pablo, J. J. *J. Chem. Phys.* **2000**, *112*, 450.
(13) Huinink, H. P.; Brokken-Zijp, J. C. M.; van Dijk, M. A.; Sevink, G. J. A. *J. Chem. Phys.* **2000**, *112*, 2452.
(14) Wang, Q.; Nealey, P. F.; de Pablo, J. J. *Macromolecules* **2001**, *34*, 3458.
(15) Sevink, G. J. A.; Zvelindovsky, A. V.; Fraaije, J.; Huinink, H. P. *J. Chem. Phys.* **2001**, *115*, 8226.
(16) Li, W. H.; Wickham, R. A.; Garbary, R. A. *Macromolecules* **2006**, *39*, 806.
(17) Yu, B.; Sun, P. C.; Chen, T. H.; Jin, Q. H.; Ding, D. T.; Li, B. H.; Shi, A. C. *J. Chem. Phys.* **2007**, *127*, 114906.
(18) He, X. H.; Song, M.; Liang, H. J.; Pan, C. Y. *J. Chem. Phys.* **2001**, *114*, 10510.
(19) Lee, J. Y.; Shou, Z. Y.; Balazs, A. C. *Macromolecules* **2003**, *36*, 7730.
(20) Suh, K. Y.; Kim, Y. S.; Lee, H. H. *J. Chem. Phys.* **1998**, *108*, 1253.
(21) Horvat, A.; Lyakhova, K. S.; Sevink, G. J. A.; Zvelindovsky, A. V.; Magerle, R. *J. Chem. Phys.* **2004**, *120*, 1117.
(22) Matsen, M. W. *Curr. Opin. Colloid Interface Sci.* **1998**, *3*, 40.
(23) Fasolka, M. J.; Mayes, A. M. *Annu. Rev. Mater. Res.* **2001**, *31*, 323.
(24) Segalman, R. A. *Mater. Sci. Eng. R* **2005**, *48*, 191.
(25) Pickett, G. T.; Balazs, A. C. *Macromol. Theory Simul.* **1998**, *7*, 249.
(26) Feng, J.; Ruckenstein, E. *Polymer* **2002**, *43*, 5775.
(27) Chen, H. Y.; Fredrickson, G. H. *J. Chem. Phys.* **2002**, *116*, 1137.
(28) Chen, P.; Liang, H. J. *J. Phys. Chem. B* **2006**, *110*, 18212.
(29) Ludwigs, S.; Krausch, G.; Magerle, R.; Zvelindovsky, A. V.; Sevink, G. J. A. *Macromolecules* **2005**, *38*, 1859.
(30) Ludwigs, S.; Schmidt, K.; Stafford, C. M.; Amis, E. J.; Fasolka, M. J.; Karim, A.; Magerle, R.; Krausch, G. *Macromolecules* **2005**, *38*, 1850.
(31) Romiszowski, P.; Sikorski, A. *J. Chem. Phys.* **2005**, *123*, 104905.
(32) Gemma, T.; Hatano, A.; Dotera, T. *Macromolecules* **2002**, *35*, 3225.
(33) Tang, P.; Qiu, F.; Zhang, H. D.; Yang, Y. L. *J. Phys. Chem. B* **2004**, *108*, 8434.
(34) He, X. H.; Huang, L.; Liang, H. J.; Pan, C. Y. *J. Chem. Phys.* **2002**, *116*, 10508.
(35) Kou, D. Z.; Jiang, Y.; Liang, H. J. *J. Phys. Chem. B* **2006**, *110*, 23557.
(36) Romiszowski, P.; Sikorski, A. *J. Mol. Model.* **2005**, *11*, 335.
(37) Drolet, F.; Fredrickson, G. H. *Phys. Rev. Lett.* **1999**, *83*, 4317.
(38) Drolet, F.; Fredrickson, G. H. *Macromolecules* **2001**, *34*, 5317.
(39) Helfand, E. *J. Chem. Phys.* **1975**, *62*, 999.
(40) Meng, D.; Wang, Q. *J. Chem. Phys.* **2007**, *126*, 234902.
(41) Khanna, V.; Cochran, E. W.; Hexemer, A.; Stein, G. E.; Fredrickson, G. H.; Kramer, E. J.; Li, X.; Wang, J.; Hahn, S. F. *Macromolecules* **2006**, *39*, 9346.
(42) Bosse, A. W.; Garcia-Cervera, C. J.; Fredrickson, G. H. *Macromolecules* **2007**, *40*, 9570.
(43) Tzeremes, G.; Rasmussen, K. O.; Lookman, T.; Saxena, A. *Phys. Rev. E* **2002**, *65*, 5.
(44) Fredrickson, G. H. *Macromolecules* **1991**, *24*, 3456.
(45) Matsen, M. W.; Schick, M. *Phys. Rev. Lett.* **1994**, *72*, 2660.
(46) Tyler, C. A.; Qin, J.; Bates, F. S.; Morse, D. C. *Macromolecules* **2007**, *40*, 4654.
(47) Guo, Z. J.; Zhang, G. J.; Qiu, F.; Zhang, H. D.; Yang, Y. L.; Shi, A. C. *Phys. Rev. Lett.* **2008**, *101*, 4.
(48) Feng, J.; Ruckenstein, E. *J. Chem. Phys.* **2007**, *126*, 124902.
(49) Yu, B.; Sun, P. C.; Chen, T. H.; Jin, Q. H.; Ding, D. T.; Li, B. H.; Shi, A. C. *J. Chem. Phys.* **2007**, *126*, 204903.
(50) Breiner, U.; Krappe, U.; Abetz, V.; Stadler, R. *Macromol. Chem. Phys.* **1997**, *198*, 1051.
(51) Sevink, G. J. A.; Zvelindovsky, A. V.; Fraaije, J. G. E. M.; Huinink, H. P. *J. Chem. Phys.* **2001**, *115*, 8226.

JP801675Z